JOURNAL OF THERMOPHYSICS AND HEAT TRANSFER
Vol. 20, No. 4, October–December 2006

Effects of Forced Convection and Surface Tension During Methanol Droplet Combustion

Vasudevan Raghavan*
University of Nebraska at Lincoln, Lincoln, Nebraska 68588-0656
Daniel N. Pope†
University of Minnesota at Duluth, Duluth, Minnesota 55812-3042
and
George Gogos‡
University of Nebraska at Lincoln, Lincoln, Nebraska 68588-0656

DOI: 10.2514/1.21174

A numerical investigation of surface tension and forced convection effects on moving and suspended methanol droplets burning in a zero-gravity, low-pressure air environment is presented. Simulations were conducted using a predictive, transient, axisymmetric model for an initial droplet diameter of 0.5 mm, an ambient temperature of 1200 K, and initial Reynolds numbers (Re_0) in the range of 1–100. Results indicate that, for moving droplets, due to the presence of an envelope flame at some stage during the droplet lifetime, surface tension is important over the range of Re_0 considered; the extinction diameter decreases with increasing Re_0. For suspended droplets, when transition or envelope flame is present (Re_0 less than approximately 15), surface tension is important; when an envelope flame is present (Re_0 less than approximately 10), the extinction diameter increases with Re_0. Both for suspended and moving droplets, the droplet lifetime is weakly sensitive to surface tension. The variation of droplet lifetimes with Re_0 is much stronger for suspended droplets than for moving droplets. Depending on the Reynolds number, results on methanol droplet lifetimes and extinction diameters measured through suspended droplet experiments may not be applicable to moving droplets.

Nomenclature

A	=	preexponential factor
a	=	fuel concentration exponent in reaction equation
b	=	oxygen concentration exponent in reaction equation
C_D	=	drag coefficient
c_p	=	specific heat
D	=	ordinary diffusion coefficient
Da	=	Damköhler number, $[A\frac{R_0}{\lvert u_\infty\rvert}\rho^{a+b-1}W_f^{1-a}(\frac{1}{W_O})^b \exp(\frac{-E_a}{R_u T_\infty})]$
D_T	=	thermal diffusion coefficient
d_0	=	initial droplet diameter
d_e	=	extinction diameter
E_a	=	activation energy
K	=	evaporation constant
k	=	thermal conductivity
L	=	latent heat of vaporization
m''_θ	=	local mass flux at the droplet surface
p	=	pressure
R	=	droplet radius
Re	=	Reynolds number ($\rho v d/\mu$)
R_u	=	universal gas constant
r	=	radial coordinate
T	=	temperature
t	=	time
u_∞	=	freestream velocity
V	=	diffusion velocity
v	=	velocity
W	=	molecular weight
Y	=	mass fraction
μ	=	viscosity
θ	=	θ-coordinate
υ'_i	=	stoichiometric coefficient of the ith species as a reactant
υ''_i	=	stoichiometric coefficient of the ith species as a product
ρ	=	density
σ	=	surface tension
ω_i	=	rate of production of ith species

Subscripts

∞	=	freestream or outer computational boundary
θ	=	polar
0	=	initial condition
f	=	fuel
g	=	gas phase
i	=	ith species
l	=	liquid phase
r	=	radial
s	=	droplet surface
w	=	water

Received 17 November 2005; revision received 2 February 2006; accepted for publication 3 February 2006.

*Post Doctoral Research Associate, Department of Mechanical Engineering, N104 Walter Scott Engineering Center.
†Assistant Professor, Department of Mechanical and Industrial Engineering, 105 Voss-Kovach Hall, 1305 Ordean Court.
‡Professor, Department of Mechanical Engineering, N104 Walter Scott Engineering Center; ggogos@unl.edu.

I. Introduction

THE use of methanol as a fuel in isolated droplet combustion experiments offers several advantages; methanol has a simple chemical composition, it does not produce soot, and its oxidation mechanism is well understood. An added complication when using methanol is the absorption of a major ambient species (water) into the droplet. This absorption of water is due to the high polarity of both water and methanol molecules that causes them to readily mix. Water initially present in the ambient and/or produced through combustion condenses on the droplet surface and is transported to the

droplet interior causing a continuous increase in water content within the droplet. The water content within the droplet eventually reaches a level where, in combination with gas-phase convection, the vaporizing methanol can no longer sustain the combustion reaction, leading to flame extinction.

Experimental studies on spherically symmetric combustion of fuel droplets have been carried out by several investigators [1–8]. These investigators either deployed the droplets without any support [1–5,8] or used thin fibers to suspend the droplets [6,7]. Both suspended and unsupported droplet experiments are often conducted in a quiescent, microgravity environment [1,2,4–8] in order to minimize the deviation from spherical symmetry. Several investigators, such as Marchese et al. [4], Shaw [9], Zhang, et al. [10] and Marchese and Dryer [11], have conducted one-dimensional analytical and numerical studies to simulate spherically symmetric methanol droplet combustion. It has been shown that considering only diffusion transport of water into the methanol droplet leads to predicted extinction diameters that are much lower than the corresponding experimental results [10,11]. Investigators concluded that internal mixing must be responsible for additional water within the droplets, which leads to much larger extinction diameters than those predicted using one-dimensional models. The sources of internal mixing in spherically symmetric droplet combustion are likely multifold, but are not due to relative gas/liquid convection effects at the interface [4]. Shaw [9] performed an asymptotic analysis and determined that water transport influences conditions in and near the flame and the burning rates of initially-pure methanol droplets. Experimental results show that the water mass content in the droplet is approximately 40 to 80% at extinction [10]. Water transport due to diffusion alone cannot account for the large quantities of water absorbed [11]. It has been suggested in the literature that surface tension gradients could be responsible for *perfect mixing* [10,11], which can account for the amount of water measured in the experiments.

Experimental studies of droplet burning under forced convection use either porous spheres or suspended droplets. In both types of experiments, the ambient oxidizer is often blown over the droplet at a fixed velocity (freestream velocity). Porous spheres have been employed by Spalding [12], Gollahalli and Brzustowski [13], Sami and Ogasawara [14], and Raghavan et al. [15]. These investigators have shown that the freestream velocity could be varied to produce three different flame configurations; the flame forms in the wake of the droplet (wake flame), the flame partially surrounds the droplet (transition flame), and the flame completely surrounds the droplet (envelope flame). The suspended droplet technique within a convective environment [16–18] takes into account transient effects such as droplet heat up, variations in flame shapes and dimensions, and the decrease of droplet diameter with time. An experimental study of moving droplets using a freely falling chamber to generate microgravity conditions was conducted by Okajima and Kumagai [19]. They have reported that for a moving droplet there is a slight reduction in the mass burning rate, as compared with a suspended droplet.

Axisymmetric numerical models have also been developed and reported in the literature. Dwyer and Sanders [20] were one of the first research teams to develop an unsteady numerical model for the moving droplet case. They predicted a transition from a wake flame to an envelope flame as the droplet velocity decreased. Aharon and Shaw [21], in their numerical investigation of a bicomponent droplet using an axisymmetric droplet evaporation model, have concluded that the thermal Marangoni effect (surface tension gradient due to temperature gradient) has a stabilizing effect and the solutal Marangoni effect (surface tension gradient due to composition gradient) has a destabilizing effect. Recently, Dwyer et al. [22–24] numerically investigated surface tension effects for both vaporizing and combusting methanol droplets with their axisymmetric model. Their results show that thermal and solutal Marangoni phenomena can have a strong effect on the flow patterns within a liquid droplet. Shih and Megaridis [25] also considered the thermal Marangoni effect on droplet evaporation in a convective environment. They have concluded that surface tension gradients due to spatial variations of temperature along the interface have a profound impact on droplet dynamic behavior. Pope and Gogos [26,27], Pope et al. [28], and Howard et al. [29] developed axisymmetric droplet combustion models and predicted quantities like extinction velocities and extinction diameters.

Howard et al. [29], in their transient study of methanol droplet combustion within a nearly quiescent environment, reported that a weak liquid-phase circulation introduced as a perturbation through a weak gas-phase convective flow ($Re = 0.01$) is greatly enhanced due to surface tension effects. The inclusion of surface tension effects creates complex flow patterns in the droplet, which aid the absorption of water by enhancing mixing within the droplet. If surface tension effects are neglected, water absorption due to diffusion alone produces an extinction diameter much smaller than obtained experimentally. It is shown that for a 0.43 mm droplet combusting in dry air the extinction diameter when surface tension effects are included is 0.11 and 0.054 mm when surface tension effects are neglected. Experimental work available in the literature [1] for a 0.43 mm droplet reported extinction diameters in the range of 0.16–0.19 mm.

The goal of the present study is to determine the effects of both surface tension and forced convection during the combustion of an isolated methanol droplet in air. A predictive, transient, two-phase, axisymmetric numerical model that includes surface tension effects is used in the present study. Results for droplets suspended in a hot airstream (constant relative velocity) and droplets moving within an ambient consisting of hot air are presented. Results for extinction diameters and droplet lifetimes over a wide range of initial Reynolds numbers, both for suspended and moving droplets, with and without the effects of surface tension, are discussed in detail. The details of the numerical model, its validation and results, along with detailed discussions are presented in the subsequent sections.

II. Numerical Model

The numerical model used in this work is an axisymmetric, transient model that solves the conservation of mass, momentum, species, and energy equations in both the gas and liquid phase. The main features of this model are the inclusion of multicomponent diffusion in both the phases, a comprehensive method to deal with the interface (including surface tension effects), and variation of thermophysical properties as a function of temperature and species concentration in both the phases. A detailed description of the model and its validation for n-heptane droplet combustion is given in Pope et al. [28]. The model has been modified for the present study to include methanol as the fuel, surface tension effects, and liquid-phase conservation of species equations. A brief description of the model and the assumptions employed are given next.

The model simulates the combustion of a liquid methanol droplet in a low-pressure, zero-gravity, convective environment of infinite expanse (Fig. 1). For the suspended droplet, the $r - \theta$ coordinate system is inertial, whereas for the moving droplet, the coordinate system is noninertial. The effect of the acceleration of the noninertial coordinate system du_∞/dt has been included in the momentum equations [28]. The freestream pressure and the freestream temperature are held constant. The effect of the suspension fiber is neglected when simulating suspended droplets. Other assumptions

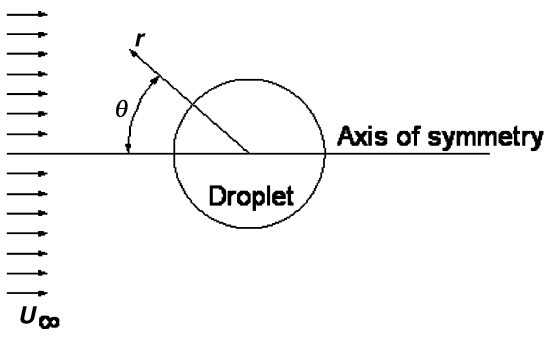

Fig. 1 Problem schematic.

include: 1) axisymmetric, laminar flow, 2) spherical droplet shape (uniform surface regression as a result of surface-averaged vaporization and surface-averaged drag force estimates have been used in order to maintain spherical droplet shape), 3) zero coefficient of bulk viscosity, and 4) negligible thermal radiation, pressure diffusion, Dufour effect, Soret effect in the liquid phase, viscous dissipation, and pressure work.

The governing equations for the gas and liquid phases are the transient axisymmetric equations for continuity, conservation of species, conservation of energy, and conservation of momentum in $r-\theta$ spherical coordinates. In the liquid phase, which consists of a binary methanol-water system, there is no production or destruction of species. A set of interfacial conservation equations couple the gas and the liquid phase.

The gas and liquid phases are constrained to have the same temperature at the interface ($T_{g,s} = T_{l,s}$). No-slip condition is employed to obtain the tangential velocities at the interface ($v_{\theta,g,s} = v_{\theta,l,s}$). The continuity of mass at the interface yields the radial velocity component v_r, given as follows

$$\rho_{g,s}[v_{r,g,s} - (dR/dt)] = \rho_{l,s}[v_{r,l,s} - (dR/dt)] \tag{1}$$

In the preceding equation dR/dt represents the droplet regression rate. Conservation of species at the interface is given by the following expressions:

fuel

$$m''_\theta Y_{f,g,s} + \rho_{g,s} Y_{f,g,s} V_{r,f,g,s} = m''_\theta Y_{f,l,s} + \rho_{l,s} Y_{f,l,s} V_{r,f,l,s} \tag{2}$$

water

$$m''_\theta Y_{w,g,s} + \rho_{g,s} Y_{w,g,s} V_{r,w,g,s} = m''_\theta Y_{w,l,s} + \rho_{l,s} Y_{w,l,s} V_{r,w,l,s} \tag{3}$$

for other species

$$m''_\theta Y_{i,g,s} + \rho_{g,s} Y_{i,g,s} V_{r,i,g,s} = 0 \tag{4}$$

Conservation of energy at the interface is given by

$$m''_\theta (Y_{f,l,s} L_f + Y_{w,l,s} L_w) + \rho_{l,s} (Y_f V_{r,f} L_f + Y_w V_{r,w} L_w)_{l,s} - k_{g,s} (dT/dr)|_{g,s} = -k_{l,s} (dT/dr)|_{l,s} \tag{5}$$

The equation for continuity of shear stress at the interface is of particular interest for the present study and includes surface tension effects. It is given by

$$\mu_{g,s}[(\partial v_\theta/\partial r) + (1/r)(\partial v_r/\partial\theta) - (v_\theta/r)]_{g,s} + (1/r)(\partial\sigma/\partial\theta)|_s = \mu_{l,s}[(\partial v_\theta/\partial r) + (1/r)(\partial v_r/\partial\theta) - (v_\theta/r)]_{l,s} \tag{6}$$

where the second term on the left-hand side is the surface tension gradient along the droplet surface. The gas-phase diffusion velocities, which depend upon concentration and temperature gradients for all N species, are solved according to the method presented by Pope and Gogos [26]. The liquid phase consists of a binary mixture of methanol and water, and the diffusion velocities are calculated using Fick's law for ordinary diffusion alone. The binary diffusion coefficient is calculated as a function of mutual binary diffusion coefficients at very low concentrations, mole fractions of the species, and a thermodynamic correction factor that depends upon composition and temperature for a binary mixture. The interface composition is determined using a low-pressure binary vapor-liquid equilibrium equation based upon the activity coefficients. The activity coefficients are calculated using the Wilson correlation [30]. Variable thermophysical properties in the gas phase are calculated using correlations from Reid et al. [31] and McBride et al. [32]. The liquid-phase properties are calculated using correlations from Reid et al. [31] as well as Teja [33] and Teja and Rice [34]. The gradient of the surface tension along the droplet surface can be expressed in terms of the surface temperature and surface water mass fraction (Y_{ws}) gradients, as follows:

$$(\partial\sigma/\partial\theta) = (\partial\sigma/\partial T_s)(\partial T_s/\partial\theta) + (\partial\sigma/\partial Y_{ws})(\partial Y_{ws}/\partial\theta) \tag{7}$$

The first term in the preceding equation represents the thermal Marangoni effect (which drives the liquid from hot to cold regions of the gas-liquid interface) and the second term represents the solutal Marangoni effect (which drives the liquid from low to high water mass fractions of the gas-liquid interface). Surface tension for a pure component (methanol or water) is calculated from a temperature dependent curve fit of experimental data [35]. A mixing rule based on composition [31] is used to yield a temperature- and composition-dependent surface tension. Thus, both the droplet surface composition and the droplet surface temperature play a role in determining surface tension. The experimental results of Santos et al. [36] for water/methanol mixtures in thermodynamic equilibrium with air at 303.15 K along with results from the code used in this study compare well.

A one-step overall reaction is used to model the combustion of methanol in air and is given next:

$$CH_3OH + 1.5(O_2 + 3.77N_2) \rightarrow CO_2 + 2H_2O + 1.5(3.77N_2) \tag{8}$$

The resulting expression for the mass-based rate of production/destruction of species I per unit volume, given by ω_i, is written as

$$\omega_i = W_i(v''_i - v'_i) A(\rho Y_f/W_f)^a (\rho Y_o/W_o)^b \exp[-E_a/R_u T] \tag{9}$$

The preexponential factor, activation energy, and the fuel and oxygen concentration exponents used in the simulation have been taken from Westbrook and Dryer [37]. Quasi-steady simulations were performed to validate the global single-step mechanism as discussed in the Model Validation section.

The governing equations are discretized using the finite volume [38] and SIMPLEC [39] methods. Convection diffusion is modeled using the power-law scheme [38]. A collocated grid is used with hyperbolic tangent stretching functions [40] used to cluster the grid points near the droplet surface in both the gas and the liquid phases. The discretized equations are solved using the alternating direction implicit (ADI) method with the tri-diagonal matrix algorithm (TDMA). Iterations are performed within each time step until desired convergence is achieved. An adaptive time step has also been employed. Grid and domain independence studies have been carried out to ensure that the solution is independent of grid and domain size. The minimum and maximum time steps have been fixed so as to capture the physics during the entire evaporation and combustion processes.

A. Model Validation

To validate the global single-step mechanism used in the present model, a few quasi-steady simulations have been carried out to simulate porous sphere experiments reported in the literature. The extinction velocities predicted by a quasi-steady version of our model have been compared with those obtained experimentally by Sami and Ogasawara [14]. Extinction velocity is defined as the freestream velocity that causes transition from an envelope flame to a wake flame. Table 1 shows the values for extinction velocity at different droplet (porous sphere) diameters. The numerical and experimental results are in good agreement, justifying the use of global single-step kinetics for the present model.

Table 1 Comparison of extinction velocity obtained from numerical and experimental results.

	Extinction velocity (m/s)	
d (mm)	Present study numerical	Sami and Ogasawara [14] experimental
5	1.01	1.18
10.1	1.57	1.49

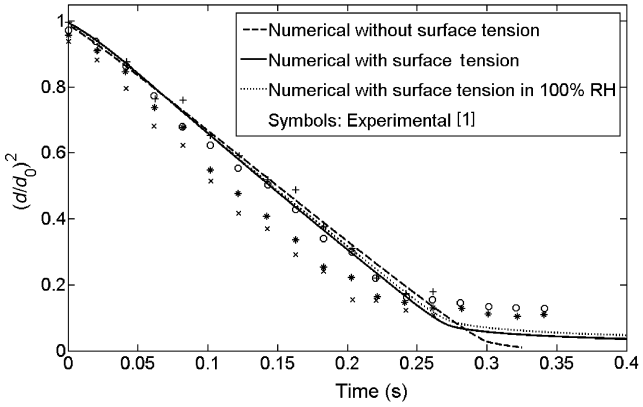

Fig. 2 Nondimensional diameter squared vs. time.

Transient simulations using the numerical code have been compared with the experimental data reported in Yang et al. [1]. The parameters for the simulations have been chosen to match those of the experimental work [1]. These simulations were conducted with an initial droplet diameter (d_0) of 0.43 mm, an ambient pressure of 1 atm, an ambient temperature of 300 K, and a droplet that is initially-pure methanol. Two cases for combustion in dry air were considered; one with surface tension effects and one without. Because the extent of air humidity has not been reported in Yang et al. [1], a third case, which includes surface tension effects and with 100% relative humidity, has also been simulated. An initial Reynolds number (based on freestream conditions and initial droplet diameter) of 0.01 has been selected to correspond to the nearly quiescent environment in the experimental work. Figure 2 shows the square of the dimensionless diameter $(d/d_0)^2$ as a function of time after ignition for the three simulations along with the experimental results [1] for four cases. Data for the three simulations have been time-shifted, so that $t = 0$ s corresponds to the end of ignition, which is when the experimental data collection begins. Figure 2 shows that all three simulations are in good agreement with the experimental data for most of the droplet lifetime and approximately follow the classical d^2-law. However, near extinction, there are differences between the numerical and experimental results. The diameter corresponding to the time when the slope of the $(d/d_0)^2$ curve drastically changes is termed the extinction diameter (d_e). Beyond this point in time, in the absence of a flame, the droplet undergoes pure evaporation. The results for d_e are shown in Table 2.

The extinction diameters for the different simulations vary greatly. The simulation neglecting surface tension effects predicts the smallest extinction diameter at 0.054 mm, followed by the simulation including surface tension effects in dry air at 0.110 mm. The largest extinction diameter of 0.125 mm corresponds to the case of surface tension and saturated ambient air. Comparing these predictions to the experimental results (an average value of 0.17 mm is reported in Yang et al. [1]), it is clear that surface tension effects greatly increase the extinction diameter leading to closer agreement with the experimental data.

The difference in the extinction diameter between the experiment and the numerical simulations that include surface tension may be due to the use of a single-step reaction in the model. Excluding radiation in the present model may also contribute to the difference. However, the initial diameter of the droplet is only 0.43 mm and the literature [4] has shown that, for methanol droplets with diameters smaller than 1.5 mm, the effect of radiation becomes negligible.

Table 2 Comparison of predicted and measured extinction diameters.

Case	Relative humidity (%)	d_e (mm)
Numerical, no surface tension	0	0.054
Numerical, surface tension	0	0.110
Numerical, surface tension	100	0.125
Experiment	Not reported	0.16–0.19

III. Results and Discussion

The numerical model was used to investigate transient methanol droplet combustion in a zero-gravity, forced-convection environment, with and without surface tension effects. To neglect surface tension effects, the second term on the left-hand side of the interfacial continuity of shear stress equation has been dropped. A methanol droplet at a uniform initial temperature of 297 K and with an initial diameter of 0.5 mm burning within air at an ambient pressure of 1 atm and an ambient temperature of 1200 K has been used in all the cases. The effect of forced convection has been analyzed by varying the initial Reynolds number from 1 to 100. Both suspended as well as moving droplets have been simulated. For suspended droplets, the freestream velocity is held constant and the droplet diameter decreases with time. In the moving droplet cases, the droplet velocity also decreases with time due to the drag force [28].

A. Flame Shapes

The primary effect of forced convection is to affect the position and shape of the flame formed after the ignition transient and the subsequent behavior of the flame after ignition. The ignition transient occurs over a very short time when compared with the droplet lifetime. It can be characterized by the following sequence of events: 1) evaporation and mixing of the fuel vapor and oxidizer, 2) ignition of the fuel vapor/oxidizer mixture downstream of the droplet, and 3) rapid establishment of the flame from the wake region to a size and flame type (envelope, transition, or wake) defined by the initial droplet velocity. At low initial air/droplet relative velocities, the residence time for the flow is much larger than the chemical reaction time, and the flame completely engulfs the droplet (envelope flame). The initial relative velocity may be increased to a point where the residence time becomes too small for the completion of the chemical reaction, and the flame becomes unsustainable in the front portion of the droplet ($\theta = 0°$). The resulting flame may partially surround the droplet (transition flame) or form in the wake of the droplet (wake flame).

Figure 3 shows the predicted temperature distribution at various times during the ignition transient for a moving droplet with initial Reynolds number $Re_0 = 10$ when surface tension effects are included. The droplet initially experiences evaporation and the fuel vapor mixes with the ambient oxidizer. Ignition occurs downstream of the droplet, forming a wake flame (Fig. 3a). In this particular case, the flame rapidly approaches the droplet (Fig. 3b), partially surrounds the droplet in a transition flame configuration (Figs. 3c and 3d), and eventually surrounds the droplet in an envelope flame configuration (Figs. 3e and 3f). The entire duration of the ignition transient for this case is approximately 3.5 ms as compared with a droplet lifetime of 273 ms for this case.

The ignition transient for the moving droplet with $Re_0 = 10$ case is not noticeably affected if surface tension effects are neglected. Surface tension effects come into play only when the flame partially surrounds the droplet in a transition flame configuration which causes nonuniform heating of the droplet surface, and therefore large temperature gradients (thermal Marangoni effect). Shortly after the formation of an envelope flame, the temperature gradients are reduced and composition gradients (solutal Marangoni effect) become dominant [29]. For $Re_0 = 10$, the change from a wake to a transition, and finally to an envelope flame occurs very rapidly. Thus, the cases with and without surface tension effects produce an envelope flame at approximately the same time ($t \approx 3.5$ ms).

The flame formed during the rapid ignition transient is affected by changes in the droplet diameter and freestream velocity over the lifetime of the droplet. As discussed by Pope et al. [28], for a constant freestream temperature, the Damköhler number is proportional to the ratio of the droplet diameter and instantaneous freestream velocity, which is the characteristic convective time scale. For a suspended droplet, the freestream velocity is constant and the droplet diameter decreases with time. Thus, the Damköhler number decreases with time for a suspended droplet. For a moving droplet, both the droplet diameter and the droplet velocity decrease with time. The numerical results for n-heptane in Pope et al. [28] show that the Damköhler

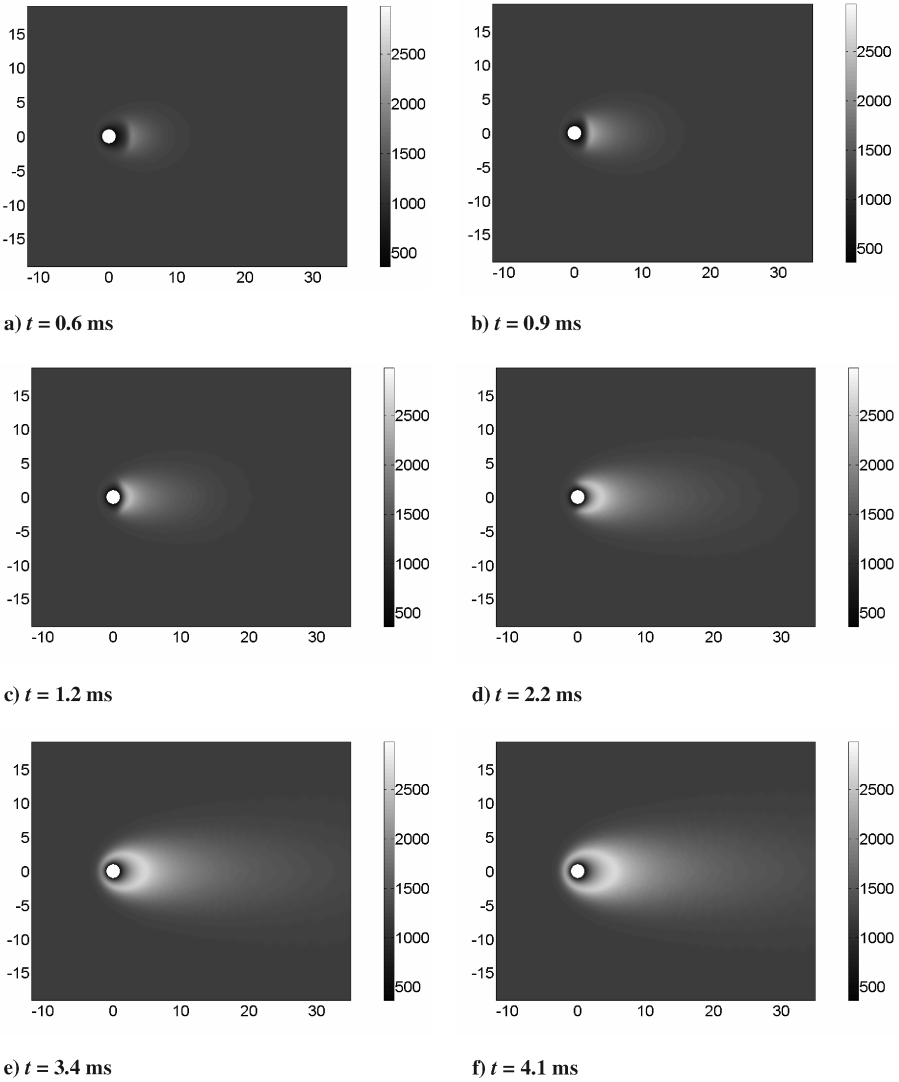

Fig. 3 Temperature distribution in Kelvin for a moving droplet ($Re_0 = 10$; with surface tension)

number increases with time for a moving droplet, which promotes the formation of an envelope flame at some point during the droplet lifetime.

B. Burning Characteristics

The current results are in qualitative agreement with the numerical results for n-heptane of Pope et al. [28]. Within the range of initial Reynolds numbers considered in the present work, an envelope flame is formed at some point during the lifetime of a moving methanol droplet. This is due to the reduction in the droplet velocity with time and the associated increase in the Damköhler number with time. For a suspended methanol droplet, an envelope flame is not observed during the lifetime of the droplet when the initial Reynolds number is approximately 15 or higher. In this range of initial Reynolds numbers, the wake flame established remains downstream for the entire droplet lifetime. To highlight the differences between the combustion characteristics of moving and suspended droplets, the temporal variations of nondimensional diameter squared $(d/d_0)^2$, Reynolds number, Damköhler number, and evaporation constant are shown in Fig. 4 for $Re_0 = 5$.

For an initial Reynolds number of 5, the suspended and moving droplets developed an envelope flame at approximately the same time ($t = 1.0$ ms). The envelope flame remained until extinction for both cases. The low Reynolds number combined with similar flame configurations results in similar time histories for both $(d/d_0)^2$ (Fig. 4a) and K (Fig. 4d). The constant velocity associated with the suspended droplet results in a higher Reynolds number (Fig. 4b) and thus a slightly higher evaporation constant (Fig. 4d). Similar experimental results indicating the evaporation constant value of a moving droplet being smaller than that of a suspended droplet have been reported in the literature [19]. Predicted trends in the Damköhler number for methanol droplets are similar to those obtained for n-heptane droplets [28], namely, the Damköhler number decreases with time for suspended droplets and increases with time for moving droplets (Fig. 4c).

Numerical predictions for moving droplets exhibit fluctuations in the variation of the Damköhler number with time during the final stages of combustion (Fig. 4c). These fluctuations will be discussed next along with Fig. 5. In the present work, the droplet lifetime t_d is defined as either the time at which extinction takes place or, for cases where the flame does not extinguish, the time at which the droplet diameter reduces to one-tenth of its initial diameter. Both the suspended and the moving droplet experienced flame extinction for the $Re_0 = 5$ case with surface tension included. For the moving droplet, t_d is 279 ms and for a suspended droplet it is 265 ms. The extinction diameter for the moving droplet case is 0.101 mm and for the suspended droplet case it is 0.113 mm (inset in Fig. 4a). At extinction, the suspended and moving droplets consist of approximately 65 and 80% water by mass, respectively. In general, both forced convection and water content inside the droplet together cause flame extinction. In the case of a moving droplet, as the droplet velocity continuously decreases, at extinction, the instantaneous Reynolds number is close to zero (approximately 0.006 for $Re_0 = 5$). Thus, the water content inside the droplet alone causes extinction for the moving droplet case. The water content inside the moving droplet

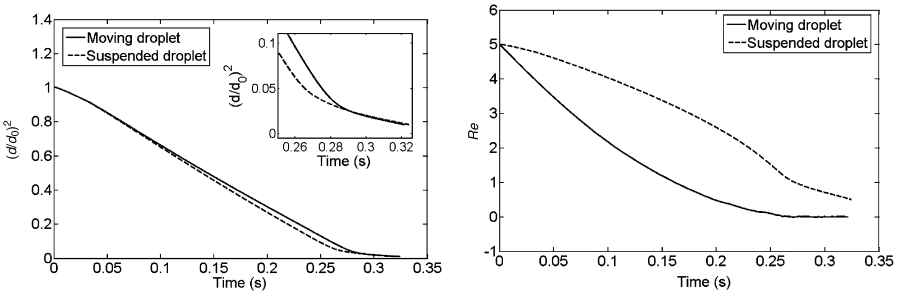

a) Time history of $(d/d_0)^2$ b) Time history of Reynolds number

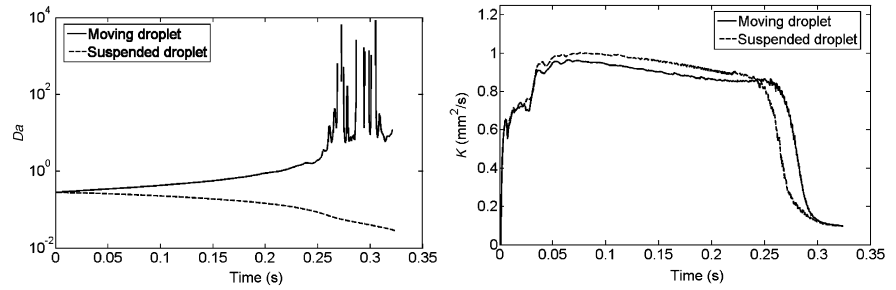

c) Time history of Damköhler number d) Time history of evaporation constant

Fig. 4 Comparison between moving and suspended droplets for $Re_0 = 5$ with surface tension.

increases to around 80% before extinction occurs. For the suspended droplet (constant relative velocity), the instantaneous Reynolds number at extinction is much larger (approximately 0.226 for $Re_0 = 5$). An early extinction occurs due to the higher convective strength associated with the suspended droplet. The water content inside the droplet is around 65% at extinction.

Figure 5 shows the time histories of the thrust drag coefficient and the droplet velocity near the end of the droplet lifetime, for a moving droplet with $Re_0 = 5$ and surface tension included. The fluctuations in the Damköhler number, shown in Fig. 4c, are due to variations in the droplet velocity (Fig. 5b). Because of velocity fluctuations about zero, the absolute value of velocity is used in the expression for the Damköhler number. Similar small oscillations are seen during the same time period, in the Reynolds number vs. time plot shown in Fig. 4b. Fluctuations in the droplet velocity occur only for the moving droplets, when their velocity is reduced considerably. These fluctuations are due to changes in the direction of the thrust drag component that the droplet experiences (Fig. 5a). The expression for the thrust drag component is given elsewhere [28].

The changes in the direction of the thrust drag component are due to variations in the radial evaporation velocity along the droplet surface. These variations produce an oscillator effect, which is explained as follows. When the droplet moves forward (say from right to left), the flame is closer to the droplet at $\theta = 0$ deg and the evaporation velocity along the front of the droplet ($\theta = 0$ deg) is higher than that along the rear of the droplet. The variation in the evaporation velocity causes a thrust force that tends to oppose the direction of motion. The droplet slows and eventually moves in the opposite direction (i.e., from left to right, shown by negative droplet velocities in Fig. 5b). Now, the flame will be closer to the droplet at $\theta = 180$ deg, causing a higher evaporation velocity along the rear of the droplet, and thus a thrust force that opposes the backward motion of the droplet. The droplet slows and eventually moves in the opposite direction. The same cycle repeats and the droplet velocity fluctuates between positive and negative values (Fig. 5b). This oscillator effect is not present earlier in the droplet lifetime when the convective strength (i.e., the Reynolds number) is high enough to damp it out.

As previously discussed, suspended droplets do not develop envelope flames for Re_0 greater than approximately 15, but moving droplets develop envelope flames at some stage during their lifetimes. The cause of this behavior is the increase and decrease of the Damköhler number with time noted for moving and suspended

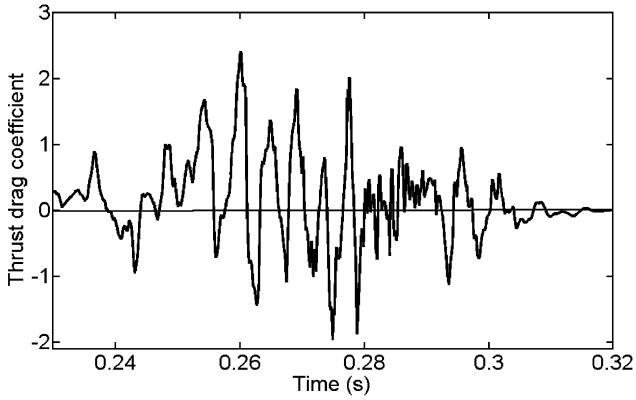

a) Thrust drag coefficient vs. time

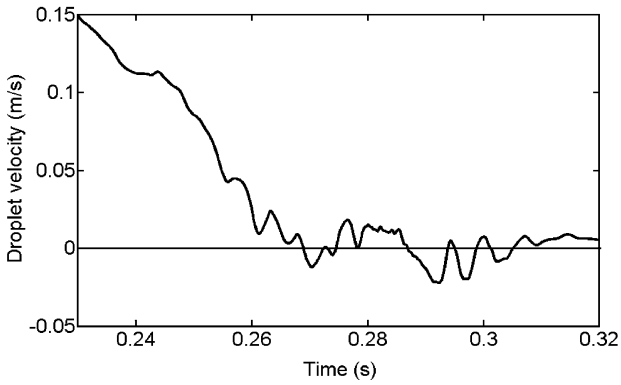

b) Droplet velocity vs. time

Fig. 5 Time histories for $Re_0 = 5$; moving droplet with surface tension effects.

droplets, respectively. Figure 6 shows the temporal variations of $(d/d_0)^2$ and K for a moving and a suspended droplet with surface tension effects included and $Re_0 = 50$. For both the suspended and the moving droplet, a wake flame is present downstream of the

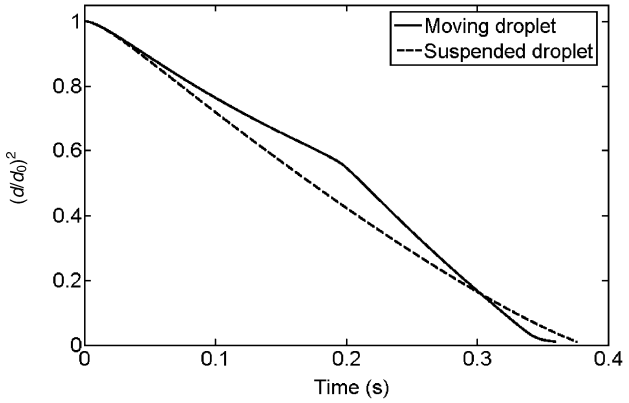

a) Time history of $(d/d_0)^2$

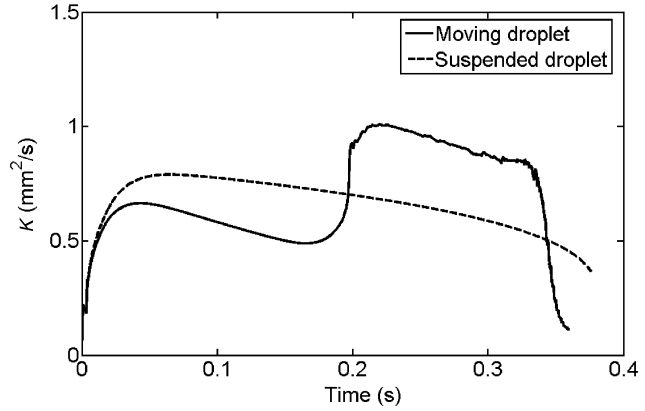

b) Time history of evaporation constant

Fig. 6 Comparison between moving and suspended droplet combustion for $Re_0 = 50$ with surface tension.

droplet after the ignition transient. The suspended droplet effectively experiences pure evaporation due to the absence of an envelope flame throughout the droplet lifetime. As a result, there is only a gradual change in the slope of the $(d/d_0)^2$ curve (Fig. 6a) and in the evaporation constant K (Fig. 6b) over time.

The simulation for the suspended droplet was stopped when the droplet diameter reached one-tenth its initial value resulting in a droplet lifetime of $t_d = 375$ ms. Similarly, the moving droplet with $Re_0 = 50$ experiences pure evaporation initially. The reduction in both droplet diameter and droplet velocity associated with the moving droplet leads to a lower K (Fig. 6b) and higher $(d/d_0)^2$ (Fig. 6a) until an envelope flame is formed at approximately $t = 198$ ms. The formation of an envelope flame is indicated by the change in slope of the $(d/d_0)^2$ curve and the rapid increase in K shown in Figs. 6a and 6b, respectively. The envelope flame supplies water vapor for absorption into the droplet. The absorption of water into the liquid droplet causes extinction ($d_e = 0.0748$ mm) and the resulting droplet lifetime is 345 ms.

C. Combustion of a Suspended Droplet

The effects of forced convection and surface tension on suspended methanol droplet combustion are presented in this section. Table 3 shows the droplet lifetimes obtained for suspended droplets at various initial Reynolds numbers when surface tension effects are both included and neglected. The variation of droplet lifetime with initial Reynolds number is also shown in Fig. 7. Both Table 3 and Fig. 7 clearly show that the droplet lifetime is weakly sensitive to surface tension, except for initial Reynolds numbers in the vicinity of $Re_0 \approx 12$. Figure 7 also shows that there are three distinct ranges of initial Reynolds numbers, where different trends of variations are seen in the droplet lifetimes with Re_0.

The first range is for Re_0 approximately less than 10. The droplet lifetime decreases with increasing initial Reynolds number. An envelope flame is established very early in the droplet lifetime (around 0.7, 1.0, 1.7, and 3.3 ms for $Re_0 = 1$, 5, 8, and 10, respectively). Flame extinction occurs for the cases shown in bold in Table 3. Droplet lifetime variation in this range is discussed extensively along with Figs. 8–10 later in this section.

The second range is approximately from $Re_0 = 10$ to 15. In this range, the droplet lifetime sharply increases with increasing initial Reynolds number, and flame transition from one flame type to another is highly unstable. Figure 11 and related discussion presented later explains the droplet lifetime variation trend in this range.

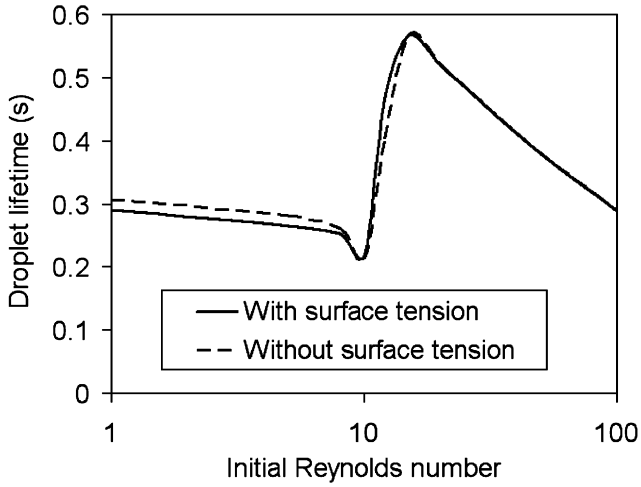

Fig. 7 Droplet lifetime for suspended droplets.

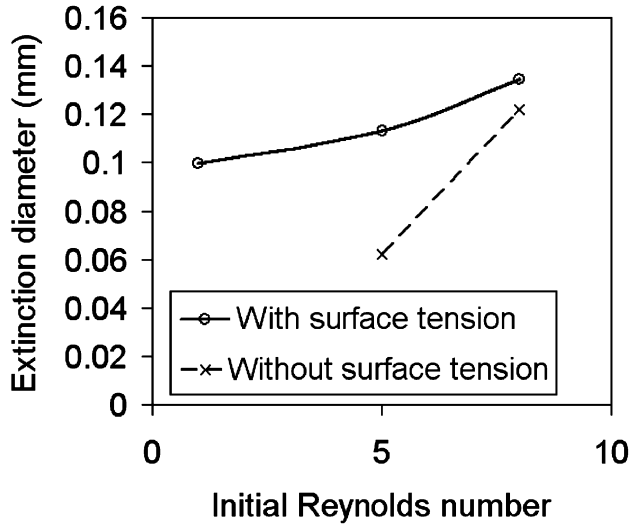

Fig. 8 Extinction diameter for suspended droplets.

Table 3 Droplet lifetimes at various initial Reynolds numbers for suspended droplets.

	Droplet lifetime t_d in seconds	
Re_0	With surface tension	Without surface tension
1	**0.291**	0.303
5	**0.265**	**0.281**
8	**0.253**	**0.261**
10	**0.219**	**0.213**
12	0.459	0.398
15	0.562	0.562
20	0.515	0.515
30	0.451	0.451
50	0.375	0.375
100	0.285	0.285

Initial Reynolds numbers greater than approximately 15 form the third range. Neither envelope flames nor flame extinction is observed for these cases. The flame is established far downstream and remains downstream for the entire droplet lifetime, although it does move towards the droplet. In this range, the increasing convective strength that accompanies an increase in Re_0 causes a decrease in the droplet lifetime.

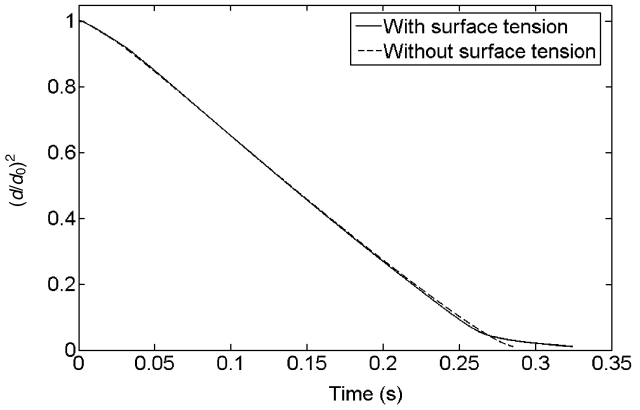

a) Time history of $(d/d_0)^2$

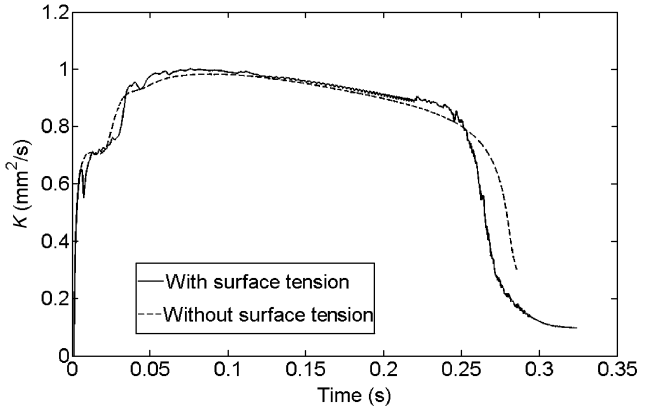

b) Time history of evaporation constant

Fig. 9 Suspended droplet combustion with and without surface tension effects for $Re_0 = 5$.

As the initial Reynolds number is increased from 1 through approximately 10 (first range in Fig. 7), the increase in the convective intensity causes an increase in the evaporation constant value (reduction in the droplet lifetime). The flame extinction diameter increases with initial Reynolds number (Fig. 8). The increase in the convective intensity is the reason for this trend.

Even though the droplet lifetimes are weakly sensitive to surface tension (Fig. 9), the extinction diameters differ between the cases that include and neglect surface tension effects. The impact of the effects of surface tension is presented in Table 4 and Fig. 10. For the case of $Re_0 = 1$ and without surface tension effects, there is no flame extinction till the diameter reached one-tenth of its initial value. Earlier extinction for the case with surface tension occurs due to enhanced water absorption. Table 4 presents the percentage of water inside the droplet at extinction for the cases with and without surface tension. It is clear from the table that the cases with surface tension effects have absorbed larger amounts of water than the cases without surface tension. The amount of water at extinction is around 60 to 80% for the case with surface tension, which is in agreement with the literature [10]. The reason for larger water absorption when the surface tension effects are included is the thorough mixing that takes place within the liquid droplet. Figure 10 shows the liquid-phase streamlines for $Re_0 = 5$ for both the cases with and without surface tension. The case without surface tension exhibits the classical Hill's vortex (Figs. 10a and 10b). However, the case with surface tension displays multicellular vortices (Figs. 10c and 10d), which lead to enhanced mixing within the liquid phase. Consequently, the inclusion of surface tension effects results in a larger amount of water absorption inside the droplet during the droplet lifetime.

For $Re_0 = 10$, the average value of the evaporation constant is nearly the same for the cases with and without surface tension ($\sim$0.92 mm^2/s). In addition, the water mass fraction inside the droplet when extinction occurs is also approximately the same (0.25) for both the cases. Because the convective intensity and mass fraction of water inside the droplet are the same, the extinction diameters are nearly equal for both the cases ($d_e = 0.205$ mm for the case with surface tension and $d_e = 0.218$ mm for the case without) for this initial Reynolds number.

The second range of initial Reynolds numbers (see Fig. 7) is between approximately 10 and 15. In this range, the droplet lifetime increases steeply with increasing initial Reynolds number. The flame

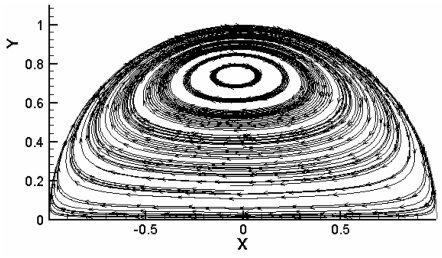

a) Without surface tension, $t \approx 6$ ms

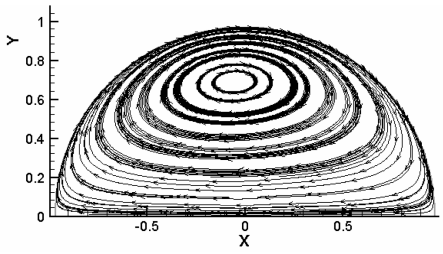

b) Without surface tension, $t \approx 24$ ms

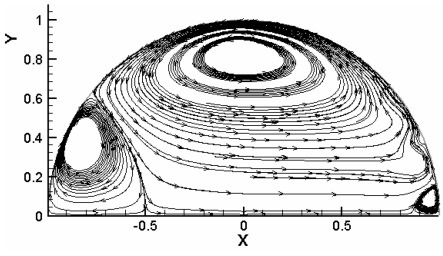

c) With surface tension, $t \approx 6$ ms

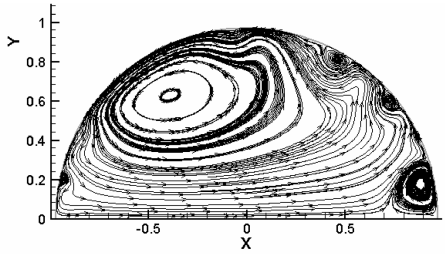

d) With surface tension, $t \approx 24$ ms

Fig. 10 Liquid-phase streamlines; suspended droplets; $Re_0 = 5$.

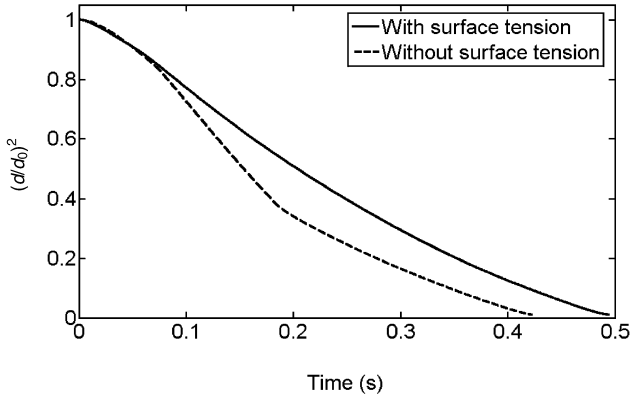

a) Time history of $(d/d_0)^2$

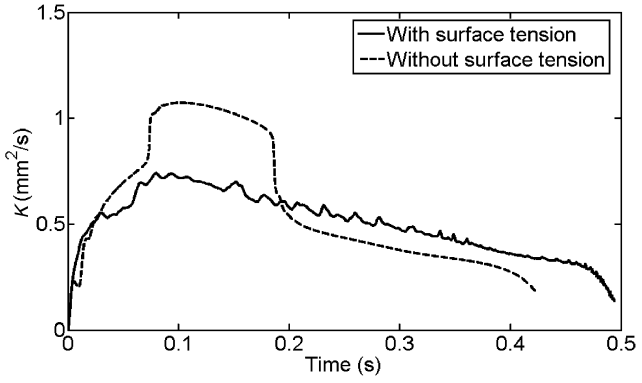

b) Time history of evaporation constant

Fig. 11 Suspended droplet combustion with and without surface tension effects for $Re_0 = 12$.

transition from one flame type to another is highly unstable. For example, at $Re_0 = 12$, the cases with and without surface tension effects displayed very different burning characteristics. A flame that partially enveloped the droplet (transition flame) is present immediately after the ignition transient for both cases. The transition flame was maintained throughout the droplet lifetime ($t_d = 0.459$ s) for the case that includes surface tension effects. However, for the case without surface tension effects, the flame evolved to an envelope flame at $t \approx 0.075$ s, changed back to a transition flame at $t \approx 0.184$ s, and remained a transition flame until the end of the droplet lifetime ($t_d = 0.398$ s). Figure 11 shows the variation of $(d/d_0)^2$ and evaporation constant K with time for $Re_0 = 12$. The $(d/d_0)^2$ curve (Fig. 11a) corresponding to the case without surface tension effects has two different slopes, one corresponding to the time period where an envelope flame existed and another when a transition flame existed. There is a smooth variation in the $(d/d_0)^2$ curve corresponding to the case with surface tension effects, where there is only a transition flame. Figure 11b shows that, when an envelope flame existed for the case without surface tension, the value of the evaporation constant is higher than the case with surface tension, producing a shorter lifetime for the case without surface tension. Thus, the initial Reynolds numbers between 10 and approximately 15 are in a transition range, where either an envelope flame never forms or if formed, it is unstable and may go back to a transition flame. Because of the instability, there is a reduction in the evaporation constant values, which eventually leads to an increased droplet lifetime in this range.

Table 4 Percentage of water inside the liquid droplet at extinction for suspended droplets at various initial Reynolds numbers.

	% of water inside the droplet at extinction	
Re_0	With surface tension	Without surface tension
1	80	30
5	65	45
8	60	40

D. Combustion of a Moving Droplet

The effects of forced convection and surface tension on moving methanol droplet combustion were also investigated. Table 5 shows the droplet lifetimes obtained for moving droplets at various initial Reynolds numbers when surface tension effects are both included and neglected.

As discussed earlier, a moving droplet develops an envelope flame at some stage of its lifetime for the entire range of the initial Reynolds numbers considered. Extinction was observed when surface tension effects were included, as indicated by the bold numerals in Table 5. The variation of extinction diameters with Re_0 is presented later in this section. For the cases that neglected surface tension effects, the flame was still present when the droplet diameter reached one-tenth of its initial value. The third column in Table 4 presents droplet lifetimes under this criterion. The fourth column presents lifetimes obtained through extrapolation to zero diameter. The variation of droplet lifetime with initial Reynolds number is also shown in Fig. 12.

The droplet lifetime t_d is weakly sensitive to surface tension effects. For both the cases that include and neglect the surface tension effect, t_d decreases with increasing Re_0 for initial Reynolds numbers in the range of 1–10, increases with Re_0 for initial Reynolds numbers in the range of 10–50, and decreases slightly for the highest initial Reynolds number considered. The droplet lifetime dependence shown in Fig. 12 will be discussed next along with Figs. 13–15.

Figure 13 shows the time history of the evaporation constant for $Re_0 = 1$ to 10. An envelope flame is established very early and surrounds the droplets for the remainder of their lifetimes. The increasing convective strength with increasing initial Reynolds number in this range causes an increase in the time-averaged value of the evaporation constant and therefore a decrease in the droplet lifetime.

Table 5 Droplet lifetime at various initial Reynolds numbers for moving droplets.

	Droplet lifetime t_d in seconds		
Re_0	With surface tension	Without surface tension	Without surface tension, lifetime extrapolated to $d = 0$
1	**0.299**	0.307	0.310
5	**0.279**	0.291	0.294
8	**0.275**	0.283	0.286
10	**0.273**	0.280	0.283
12	**0.274**	0.283	0.286
15	**0.291**	0.297	0.300
20	**0.313**	0.320	0.323
30	**0.336**	0.341	0.344
50	**0.345**	0.351	0.354
100	**0.341**	0.344	0.347

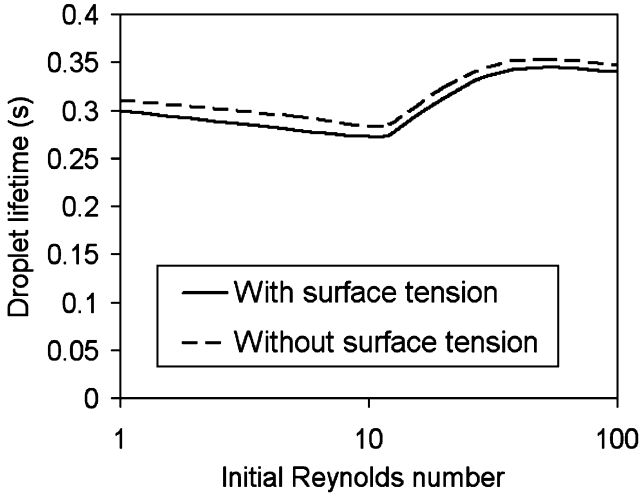

Fig. 12 Droplet lifetime for moving droplets.

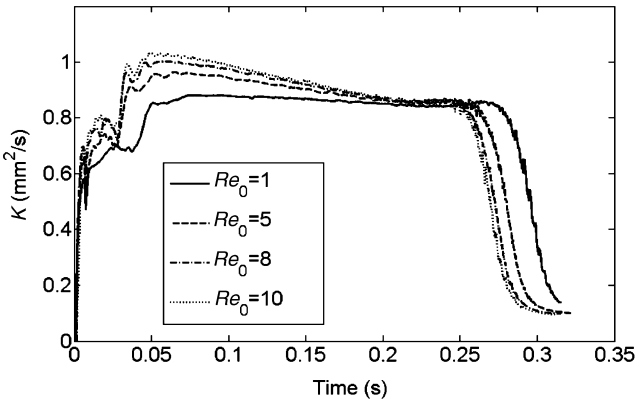

Fig. 13 Time history of K for a moving droplet with surface tension.

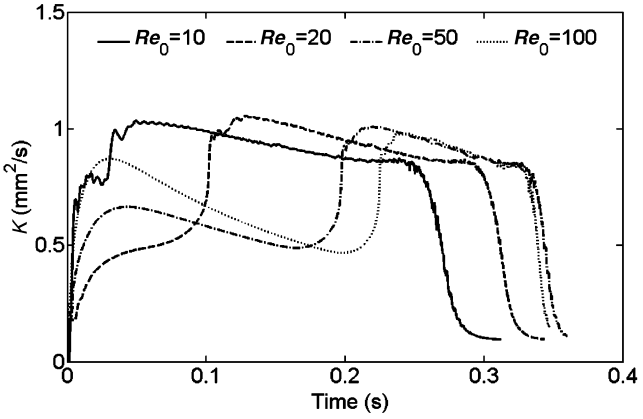

Fig. 14 Time history of the K for a moving droplet with surface tension.

For moving droplets with initial Reynolds numbers greater than 10, an envelope flame is not readily established and the droplet must decelerate before an envelope flame is formed. Figure 14 shows the time history of the evaporation constant for this range ($Re_0 =$ 10–100). It is clear from Fig. 14 that for $Re_0 > 10$, the evaporation constant sharply increases only after an envelope flame is formed. With increasing initial Reynolds number, a moving droplet spends a decreasing fraction of its lifetime surrounded by an envelope flame (Fig. 15). As a result, the time-averaged value of the evaporation constant decreases with increasing initial Reynolds number and plateaus at $Re_0 = 100$.

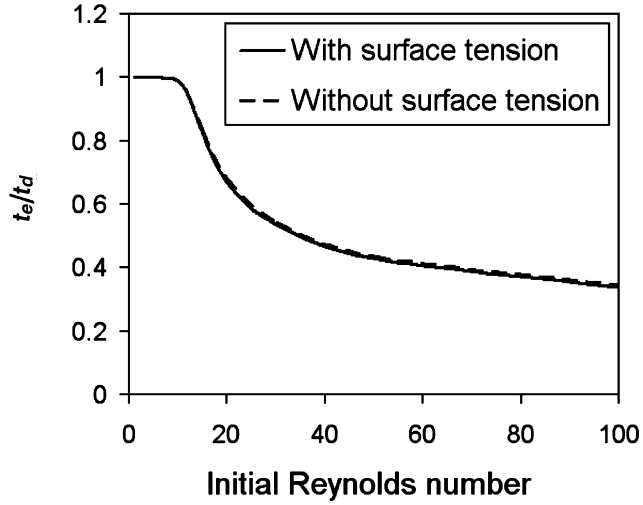

Fig. 15 Time with an envelope flame t_e/droplet lifetime t_d vs. Re_0.

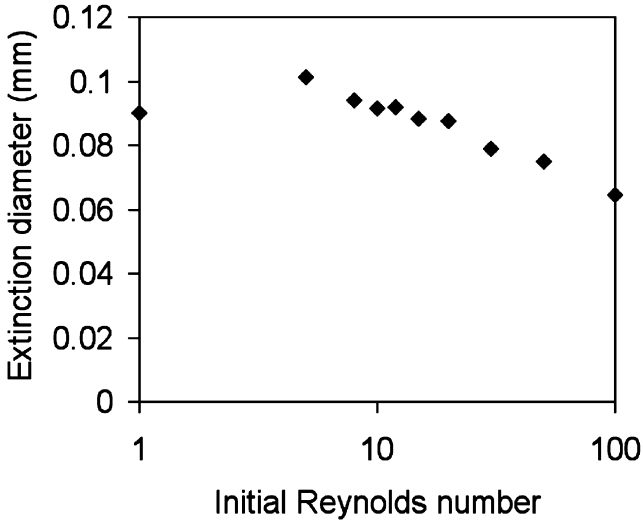

Fig. 16 Extinction diameter; moving droplet with surface tension.

Figure 16 shows the variation of extinction diameter with initial Reynolds number for a moving droplet with surface tension effects. With the exception of $Re_0 = 1$, the extinction diameter decreases with Re_0. Extinction is not observed for a moving droplet when surface tension effects are neglected; the flame is still present when the droplet diameter reaches one-tenth of its initial value.

E. Water Absorption

The water absorbed by moving and suspended droplets was also investigated. It was discussed earlier that including surface tension effects leads to more water absorbed within the liquid droplet during its lifetime (Table 4). In this section, predictions for water absorption both for moving and suspended droplets with surface tension effects are presented.

Figure 17 shows the average water mass fraction in the droplet vs. time for both a moving and a suspended droplet with an initial Reynolds number of 10. Both cases shown in Fig. 17 developed envelope flames at approximately the same time ($t \approx 3.3$ ms). It is clearly shown that, for moving droplets, surface tension effects greatly enhance water absorption. The water by mass at extinction (indicated by a vertical line) is around 85%. For the suspended droplet, the water mass fraction at extinction is approximately 0.25. For both cases, the water mass fraction within the droplet increases steadily after extinction due to preferential vaporization of the more volatile fuel species.

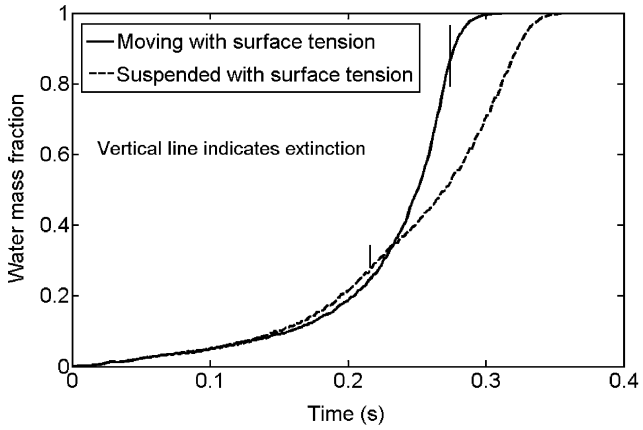

Fig. 17 Average water mass fraction in droplet; $Re_0 = 10$.

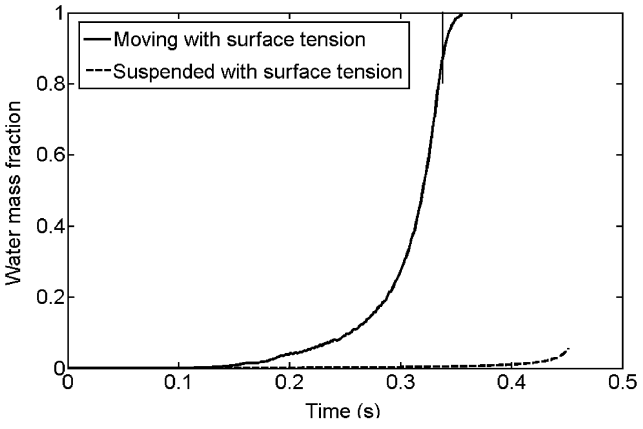

Fig. 18 Average water mass fraction within droplet; $Re_0 = 30$.

Figure 18 shows the water mass fraction within the droplet versus time for $Re_0 = 30$, for both moving and suspended droplets with surface tension effects. For the moving droplet, there is very little water absorption before the formation of an envelope flame at approximately $t = 0.15$ s. After an envelope flame is formed, the water mass fraction inside the droplet increases with time. The moving droplet consists of approximately 80% water by mass at extinction. For the suspended droplet, a small amount of water is absorbed because no envelope flame is present during the droplet lifetime. The water that is absorbed is transported from the wake flame downstream of the droplet to the droplet surface via a combination of molecular diffusion and convective transport in the recirculating wake region.

The effect of surface tension on moving methanol droplet combustion is noticeable even at the highest initial Reynolds number considered ($Re_0 = 100$). After the formation of an envelope flame at approximately $t = 220$ ms, there is a steep increase in the water absorption by the droplet when surface tension effects are included. In this case also, at extinction, water constitutes approximately 80% of the droplet mass, in agreement with the literature [10]. For the suspended droplet with $Re_0 = 100$, the wake flame formed far downstream of the suspended droplet, and thus no water was absorbed.

IV. Conclusion

The effect of surface tension and forced convection on the combustion of methanol droplets was studied using a predictive, transient, axisymmetric numerical model. Numerical results were presented for both suspended droplets (constant relative velocity) and for moving droplets with initial Reynolds numbers in the range of 1–100.

The numerical results indicate that surface tension effects are important for moving methanol droplet combustion over the entire range of initial Reynolds numbers considered. Including surface tension effects enhanced the absorption of water into the droplet which led to flame extinction. When surface tension effects were neglected, the flame surrounding a moving droplet did not extinguish. For suspended methanol droplets, surface tension effects were only important when the initial Reynolds number was less than approximately 15.

A moving droplet developed an envelope flame at some stage of its lifetime for the entire range of initial Reynolds numbers considered. With increasing initial Reynolds number, a moving droplet spends a decreasing fraction of its lifetime surrounded by an envelope flame. An envelope flame was present for suspended droplets with initial Reynolds numbers approximately less than 10. With the exception of $Re_0 = 1$, for moving droplets that include surface tension effects, the extinction diameter decreased with increasing initial Reynolds number. In contrast, the extinction diameter for suspended droplets, predicted only for Re_0 approximately less than 10, increases with initial Reynolds number. Figure 19 summarizes the extinction diameter dependence with the initial Reynolds number for suspended and moving droplets with surface tension effects. Both for suspended and moving droplets, the droplet lifetime is weakly sensitive to surface tension effects. However, the lifetime of suspended droplets exhibits a much stronger variation with initial Reynolds number than does the lifetime of moving droplets (Fig. 20).

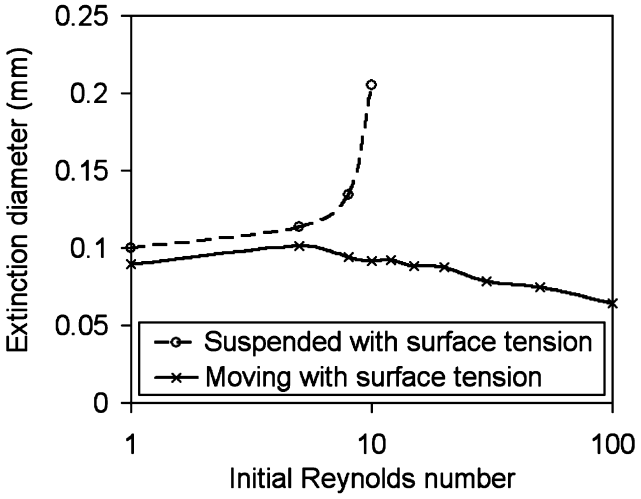

Fig. 19 Extinction diameter.

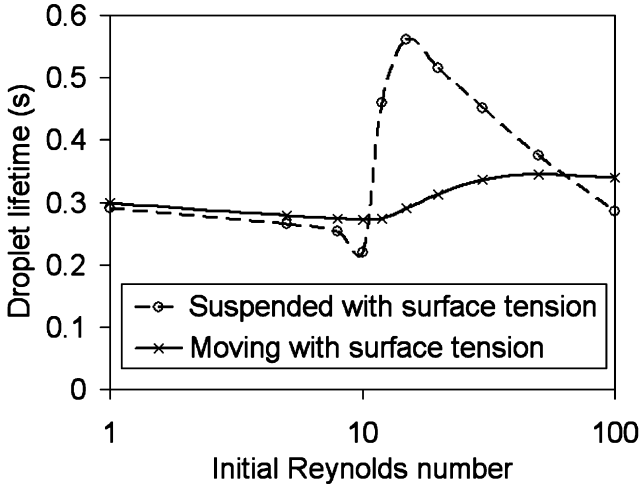

Fig. 20 Droplet lifetime.

Acknowledgements

This research was funded by NASA EPSCoR under grant NCC5-572. Computational resources were provided by the Thermal-Fluids computational facility and the Research Computing Facility at the University of Nebraska at Lincoln.

References

[1] Yang, J. C., Jackson, G. S., and Avedisian, C. T., "Combustion of Unsupported Methanol/Dodecanol Mixture Droplets at Low Gravity," *Proceedings of the Combustion Institute*, Vol. 23, The Combustion Institute, Pittsburgh, PA, 1990, pp. 1619–1625.

[2] Cho, S. Y., Choi, M. Y., and Dryer, F. L., "Extinction of a Free Methanol Droplet in Microgravity," *Proceedings of the Combustion Institute*, Vol. 23, The Combustion Institute, Pittsburgh, PA, 1990, pp. 1611–1617.

[3] Lee, A., and Law, C. K., "An Experimental Investigation on the Vaporization and Combustion of Methanol and Ethanol Droplets," *Combustion Science and Technology*, Vol. 86, 1992, pp. 235–265.

[4] Marchese, A. J., Dryer, F. L., Colantonio, R. O., and Nayagam, V., "Microgravity Combustion of Methanol and Methanol/Water Droplets: Drop Tower Experiments and Model Predictions," *Proceedings of the Combustion Institute*, Vol. 26, The Combustion Institute, Pittsburgh, PA, 1996, pp. 1209–1217.

[5] Choi, M. Y., Cho, S. Y., Dryer, F. L., and Haggard, J. B., "Some Observations on the Burning of Methanol Droplets in Microgravity Using Various Inert Gases," The Combustion Institute, Eastern States Section Meeting, Paper 73, 1998.

[6] Dietrich, D. L., Haggard, J. B., Jr., Dryer, F. L., Nayagam, V., Shaw, B. D., and Williams, F. A., "Droplet Combustion Experiments in Space Lab," *Proceedings of the Combustion Institute*, Vol. 26, The Combustion Institute, Pittsburgh, PA, 1996, pp. 1201–1207.

[7] Okai, K., Moriue, O., Araki, M., Tsue, M., Kono, M., Sato, J., Dietrich, D. L., and Williams, F. A., "Pressure Effects on Combustion of Methanol and Methanol/Dodecanol Single Droplets and Droplet Pairs in Microgravity," *Combustion and Flame*, Vol. 121, No. 3, 2000, pp. 501–512.

[8] Hara, H., and Kumagai, S., "The Effect of Initial Diameter on Free Droplet Combustion with Spherical Flame," *Proceedings of the Combustion Institute*, Vol. 25, The Combustion Institute, Pittsburgh, PA, 1994, pp. 423–430.

[9] Shaw, B. D., "Studies of Influences of Liquid-Phase Species Diffusion on Spherically Symmetric Combustion of Miscible Binary Droplets," *Combustion and Flame*, Vol. 81, Nos. 3–4, 1990, pp. 277–288.

[10] Zhang, B. L., Card, J. M., and Williams, F. A., "Application of Rate-Ratio Asymptotics to the Prediction of Extinction for Methanol Droplet Combustion," *Combustion and Flame*, Vol. 105, No. 3, 1996, pp. 267–290.

[11] Marchese, A. J., and Dryer, F. L., "The Effect of Liquid Mass Transport on the Combustion and Extinction of Bi-Component Droplets of Methanol and Water," *Combustion and Flame*, Vol. 105, Nos. 1–2, 1996, pp. 104–122.

[12] Spalding, D. B., "Experiments on the Burning and Extinction of Liquid Fuel Spheres," *Fuel*, Vol. 32, 1953, pp. 169–185.

[13] Gollahalli, S. R., and Brzustowski, T. A., "The Effect of Pressure on the Flame Structure in the Wake of a Burning Hydrocarbon Droplet," *Proceedings of the Combustion Institute*, Vol. 15, The Combustion Institute, Pittsburgh, PA, 1975, pp. 409–417.

[14] Sami, H., and Ogasawara, M., "Study on the Burning of a Fuel Drop in Heated and Pressurized Air Stream," *Bulletin of the JSME*, Vol. 13, No. 57, 1970, pp. 395–404.

[15] Raghavan, V., Babu, V., Sundararajan, T., and Natarajan, R., "Flame Shapes and Burning Rates of Spherical Fuel Particles in a Mixed Convective Environment," *International Journal of Heat and Mass Transfer*, Vol. 48, Nos. 25–26, 2005, pp. 5354–5370.

[16] Okajima, S., and Kumagai, S., "Experimental Studies on Combustion of Fuel Droplets in Flowing Air Under Zero- and High-Gravity Conditions," *Proceedings of the Combustion Institute*, Vol. 19, The Combustion Institute, Pittsburgh, PA, 1982, pp. 1021–1027.

[17] Nayagam, V., Hicks, M. C., Ackerman, M., Haggard, J. B., Jr., and Williams, F. A., "Droplet Combustion in a Slow Convective Flow," *Seventh International Microgravity Combustion Workshop*, NASA, CP 2003-212376, 2003, pp. 157–160.

[18] Gokalp, I., Chauveau, C., Richard, J. R., Kramer, M., and Leuckel, W., "Observations on the Low Temperature Vaporization and Envelope or Wake Flame Burning of n-Heptane Droplets at Reduced Gravity," *Proceedings of the Combustion Institute*, Vol. 22, The Combustion Institute, Pittsburgh, PA, 1988, pp. 2027–2035.

[19] Okajima, S., and Kumagai, S., "Further Investigations of Combustion of Free Droplets in a Freely Falling Chamber Including Moving Droplets," *Proceedings of the Combustion Institute*, Vol. 15, The Combustion Institute, Pittsburgh, PA, 1975, pp. 401–407.

[20] Dwyer, H. A., and Sanders, B. R., "Calculations of Unsteady Reacting Droplet Flows," *Proceedings of the Combustion Institute*, Vol. 22, The Combustion Institute, Pittsburgh, PA, 1988, pp. 1923–1929.

[21] Aharon, I., and Shaw, B. D., "Marangoni Instability of Bi-Component Droplet Gasification," *Physics of Fluids*, Vol. 8, No. 7, 1996, pp. 1820–1827.

[22] Dwyer, H. A., Aharon, I., Shaw, B. D., and Niazmand, H., "Surface Tension Influences on Methanol Droplet Vaporization in the Presence of Water," *Proceedings of the Combustion Institute*, Vol. 26, The Combustion Institute, Pittsburgh, PA, 1996, pp. 1613–1619.

[23] Dwyer, H. A., Shaw, B. D., and Niazmand, H., "Droplet/Flame Interactions Including Surface Tension Influences," *Proceedings of the Combustion Institute*, Vol. 27, The Combustion Institute, Pittsburgh, PA, 1998, pp. 1951–1957.

[24] Dwyer, H. A., and Shaw, B. D., "Marangoni and Stability Studies on Fiber-Supported Methanol Droplets Evaporating in Reduced Gravity," *Combustion Science and Technology*, Vol. 162, 2001, pp. 331–346.

[25] Shih, A. T., and Megaridis, C. M., "Thermocapillary Flow Effects on Convective Droplet Evaporation," *International Journal of Heat and Mass Transfer*, Vol. 39, No. 2, 1996, pp. 247–257.

[26] Pope, D. N., and Gogos, G., "A New Multi-Component Diffusion Formulation for the Finite Volume Method: Application to Convective Droplet Combustion," *Numerical Heat Transfer, Part B, Fundamentals*, Vol. 48, No. 3, 2005, pp. 213–234.

[27] Pope, D. N., and Gogos, G., "Numerical Simulation of Fuel Droplet Extinction Due to Forced Convection," *Combustion and Flame*, Vol. 142, Nos. 1–2, 2005, pp. 89–106.

[28] Pope, D. N., Howard, D., Lu, K., and Gogos, G., "Combustion of Moving Droplets and Suspended Droplets: Transient Numerical Results," *Journal of Thermophysics and Heat Transfer*, Vol. 19, No. 3, 2005, pp. 273–281.

[29] Howard, D., Pope, D. N., and Gogos, G., "Surface Tension Effects During Methanol Droplet Combustion," Drexel Univ., Paper D34, Philadelphia, 2005.

[30] Kurihara, K., Nakamichi, M., and Kojima, K., "Isobaric Vapor-Liquid Equilibria for the Methanol + Ethanol + Water and the Three Constituent Binary Systems," *Journal of Chemical and Engineering Data*, Vol. 38, 1993, pp. 446–449.

[31] Reid, R. C., Prausnitz, J. M., and Poling, B. E., *The Properties of Gases and Liquids*, McGraw–Hill, New York, 1987.

[32] McBride, B. J., Sanford, G., and Reno, M. A., "Coefficients for Calculating Thermodynamic and Transport Properties of Individual Species," NASA, TM 4513, 1993.

[33] Teja, A. S., "Simple Method for the Calculation of Heat Capacities of Liquid Mixtures," *Journal of Chemical and Engineering Data*, Vol. 28, 1983, pp. 83–85.

[34] Teja, A. S., and Rice, P., "Generalized Corresponding States Method for the Viscosities of Liquid Mixtures," *Industrial & Engineering Chemistry Fundamentals*, Vol. 20, No. 1, 1981, pp. 77–81.

[35] Vargaftik, N. B., Vinogradov, Y. K., and Yargin, V. S., *Handbook of Physical Properties of Liquids and Gases: Pure Substances and Mixture*, Begell House, New York, 1996.

[36] Santos, B. M. S., Ferriera, A., G. M., and Fonseca, I. M. A., "Surface and Interfacial Tensions of the Systems Water + n-Butyl Acetate + Methanol and Water, + n-Pentyl Acetate + Methanol at 303.15K," *Fluid Phase Equilibria*, Vol. 208, 2003, pp. 1–21.

[37] Westbrook, C. H., and Dryer, F. L., "Simplified Reaction Mechanisms for the Oxidation of Hydrocarbon Fuels in Flames," *Combustion Science and Technology*, Vol. 27, 1981, pp. 31–43.

[38] Patankar, S. V., *Numerical Heat Transfer and Fluid Flow*, Hemisphere, New York, 1980.

[39] Van Doormal, J. P., and Raithby, G. D., "Enhancements of the SIMPLE Method for Predicting Incompressible Fluid Flows," *Numerical Heat Transfer*, Vol. 7, 1984, pp. 147–163.

[40] Vinokur, M., "On One-Dimensional Stretching Functions for Finite-Difference Calculations," *Journal of Computational Physics*, Vol. 50, 1983, pp. 215–234.